Electronic Supplementary Material (ESI) for Materials Advances.

Supporting Information

Versatile synthesis of sub 10 nm sized metal-doped $M_xCo_{3-x}O_4$ nanoparticles and their electrocatalytic OER activity

Carsten Placke-Yan,[a] Georg Bendt,[a] Soma Salamon (ORCID 0000-0002-8661-6038),[b] Joachim Landers (ORCID 0000-0002-4506-6383),[b] Heiko Wende (ORCID ID: 0000-0001-8395-3541),[b] Ulrich Hagemann,[c] and Stephan Schulz[a,c] (ORCID ID: 0000-0003-2896-4488)*

[a] Institute for Inorganic Chemistry, Universitätsstraße 5-7, D-45141 Essen, Germany. E-mail: Stephan.schulz@uni-due.de

[b] Faculty of Physics and Center for Nanointegration Duisburg-Essen (CENIDE), University of Duisburg-Essen, Lotharstr. 1, D-47057 Duisburg, Germany

[c] Center for Nanointegration Duisburg-Essen (CENIDE), University of Duisburg-Essen, Carl-Benz-Straße 199, 47057 Duisburg, Germany

Content

I. Sample Preparation and Characterization

Table S1. Overview of Sample Characterization (TEM and and electrocatalytic activity parameters)

Table S2. Weights for the different doped and undoped nanoparticle samples.

II. PXRD characterization

Figure S1. PXRD measurements of S:Al005, S:Al01, S:Al02, S:0 and S:0c.

Figure S2. PXRD measurements of doped nanoparticles.

III. XPS measurements

Figure S3. XPS measurements of S:0 (a) and S:0c (b). Inset: Magnification of Co 2p.

IV. FT-IR spectroscopy

Figure S4. FT-IR measurements of uncalcinated samples S:0, S:Al005, S:Al01 and S:Al02 compared to oleylamine.

Figure S5. FT-IR measurements of calcinated nanoparticles S:0c, S:Al005c, S:Al01c and S:Al02c.

V. TEM Characterization

Figure S6-S12. TEM image and particle size distribution of metal-doped Co_3O_4 nanoparticles.

VI. EDX Characterization

Table S3. Metal concentration within the $M_{0.05}Co_{2.95}O_4$, $M_{0.1}Co_{2.9}O_4$ and $M_{0.2}Co_{2.8}O_4$ (M = Al, V, Cr, Mn, Fe, Ni) nanoparticle series determined by SEM-EDX bulk measurements.

Figure S13-18. TEM-EDX Mapping of the M-doped nanoparticle sample M02.

VII. Mössbauer spectroscopy

Figure S19. Mössbauer spectra of Fe-doped nanoparticles recorded between 5 and 300 K.

VIII. Electrochemical Characterization

Figure S20. Electrochemical characterization of doped nanoparticles in comparison with pristine Co_3O_4 consisting of LSV measurements, Tafel slope and EIS measurements.

IX. References

I. Sample Preparation and Characterization

Table S1. Overview of Sample Characterization (TEM size and electrocatalytic activity parameters)

Sample	Stoichiometry	Size (TEM) [nm]	Overpotential [mV]	Tafel slope [mV dec^{-1}]
S:0c	Co_3O_4	8.9 ± 2.4	471 ± 7	52.3
S:Al005c	$Al_{0.05}Co_{2.95}O_4$	8.3 ± 1.9	483 ± 1	57.8
S:Al01c	$Al_{0.1}Co_{2.9}O_4$	8.9 ± 1.9	492 ± 1	59.8
S:Al02c	$Al_{0.2}Co_{2.8}O_4$	9.1 ± 2.6	502 ± 6	59.9
S:V005c	$V_{0.05}Co_{2.95}O_4$	9.3 ± 2.3	464 ± 4	51.7
S:V01c	$V_{0.1}Co_{2.9}O_4$	8.6 ± 1.9	453 ± 3	50.7
S:V02c	$V_{0.2}Co_{2.8}O_4$	8.1 ± 2.2	441 ± 3	52.8
S:Cr005c	$Cr_{0.05}Co_{2.95}O_4$	7.9 ± 1.9	464 ± 4	54.1
S:Cr01c	$Cr_{0.1}Co_{2.9}O_4$	9.2 ± 2.2	457 ± 3	52.6
S:Cr02c	$Cr_{0.2}Co_{2.8}O_4$	9.1 ± 2.4	438 ± 5	49.2
S:Mn005c	$Mn_{0.05}Co_{2.95}O_4$	8.0 ± 2.0	472 ± 4	43.1
S:Mn01c	$Mn_{0.1}Co_{2.9}O_4$	7.5 ± 2.0	485 ± 5	50.1
S:Mn02c	$Mn_{0.2}Co_{2.8}O_4$	8.2 ± 2.7	490 ± 10	53.6
S:Fe005c	$Fe_{0.05}Co_{2.95}O_4$	7.3 ± 2.4	474 ± 9	50.3
S:Fe01c	$Fe_{0.1}Co_{2.9}O_4$	7.7 ± 2.2	460 ± 6	54.0
S:Fe02c	$Fe_{0.2}Co_{2.8}O_4$	8.0 ± 2.9	445 ± 11	49.6
S:Ni005c	$Ni_{0.05}Co_{2.95}O_4$	9.0 ± 1.7	476 ± 7	50.5
S:Ni01c	$Ni_{0.1}Co_{2.9}O_4$	8.6 ± 2.8	469 ± 3	49.0
S:Ni02c	$Ni_{0.2}Co_{2.8}O_4$	9.6 ± 2.9	461 ± 6	46.4

Table S2. Amounts for the different doped and undoped nanoparticle samples.

Sample	Stoichiometry	n($Co(acac)_2$) [mmol]	m($Co(acac)_2$) [g]	Dopant-Source	n(Dopant) [mmol]	m(Dopant) [mg]
S:0c	Co_3O_4	7.500	1.928	-	-	-
S:Al005c	$Al_{0.05}Co_{2.95}O_4$	7.375	1.896	$Al(acac)_3$	0.125	40.5
S:Al01c	$Al_{0.1}Co_{2.9}O_4$	7.250	1.860	$Al(acac)_3$	0.250	81.1
S:Al02c	$Al_{0.2}Co_{2.8}O_4$	7.000	1.800	$Al(acac)_3$	0.500	162.2
S:V005c	$V_{0.05}Co_{2.95}O_4$	7.375	1.896	$V(acac)_3$	0.125	43.5
S:V01c	$V_{0.1}Co_{2.9}O_4$	7.250	1.860	$V(acac)_3$	0.250	87.1
S:V02c	$V_{0.2}Co_{2.8}O_4$	7.000	1.800	$V(acac)_3$	0.500	174.1
S:Cr005c	$Cr_{0.05}Co_{2.95}O_4$	7.375	1.896	$Cr(NO_3)_3 \cdot 9H_2O$	0.125	50.0
S:Cr01c	$Cr_{0.1}Co_{2.9}O_4$	7.250	1.860	$Cr(NO_3)_3 \cdot 9H_2O$	0.250	100.1
S:Cr02c	$Cr_{0.2}Co_{2.8}O_4$	7.000	1.800	$Cr(NO_3)_3 \cdot 9H_2O$	0.500	200.1
S:Mn005c	$Mn_{0.05}Co_{2.95}O_4$	7.375	1.896	$Mn(acac)_2$	0.125	31.6
S:Mn01c	$Mn_{0.1}Co_{2.9}O_4$	7.250	1.860	$Mn(acac)_2$	0.250	63.3
S:Mn02c	$Mn_{0.2}Co_{2.8}O_4$	7.000	1.800	$Mn(acac)_2$	0.500	126.6
S:Fe005c	$Fe_{0.05}Co_{2.95}O_4$	7.375	1.896	$Fe(acac)_3$	0.125	44.1
S:Fe01c	$Fe_{0.1}Co_{2.9}O_4$	7.250	1.860	$Fe(acac)_3$	0.250	88.3
S:Fe02c	$Fe_{0.2}Co_{2.8}O_4$	7.000	1.800	$Fe(acac)_3$	0.500	176.6
S:Ni005c	$Ni_{0.05}Co_{2.95}O_4$	7.375	1.896	$Ni(acac)_2$	0.125	32.1
S:Ni01c	$Ni_{0.1}Co_{2.9}O_4$	7.250	1.860	$Ni(acac)_2$	0.250	64.2
S:Ni02c	$Ni_{0.2}Co_{2.8}O_4$	7.000	1.800	$Ni(acac)_2$	0.500	128.5

II. PXRD characterization

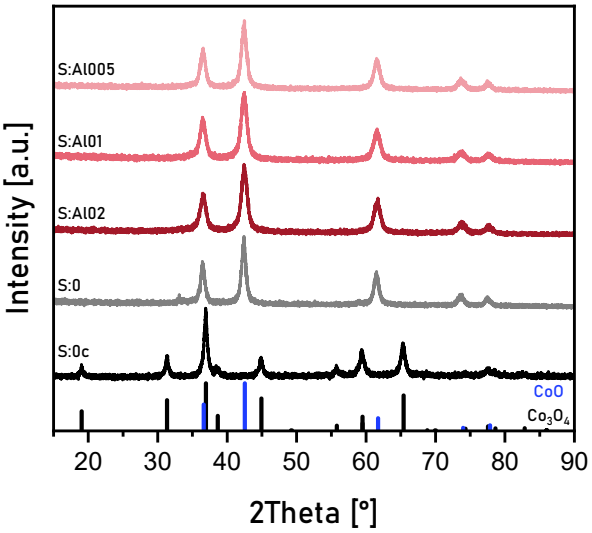

Figure S1. PXRD measurements of S:Al005, S:Al01, S:Al02, S:0 and S0c. Reference diffractograms for CoO (PDF 01-074-2391, blue) and Co_3O_4 (PDF 01-076-1802, black).

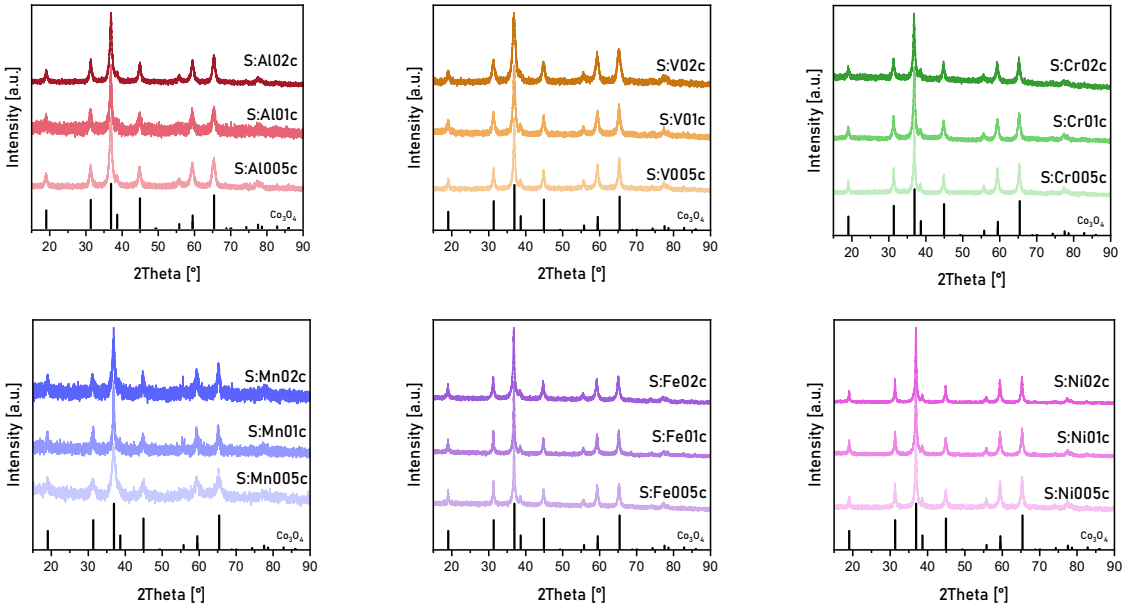

Figure S2. PXRD measurements of doped nanoparticles. Reference diffractogram for Co_3O_4 (PDF 01-076-1802).

III. XPS measurements

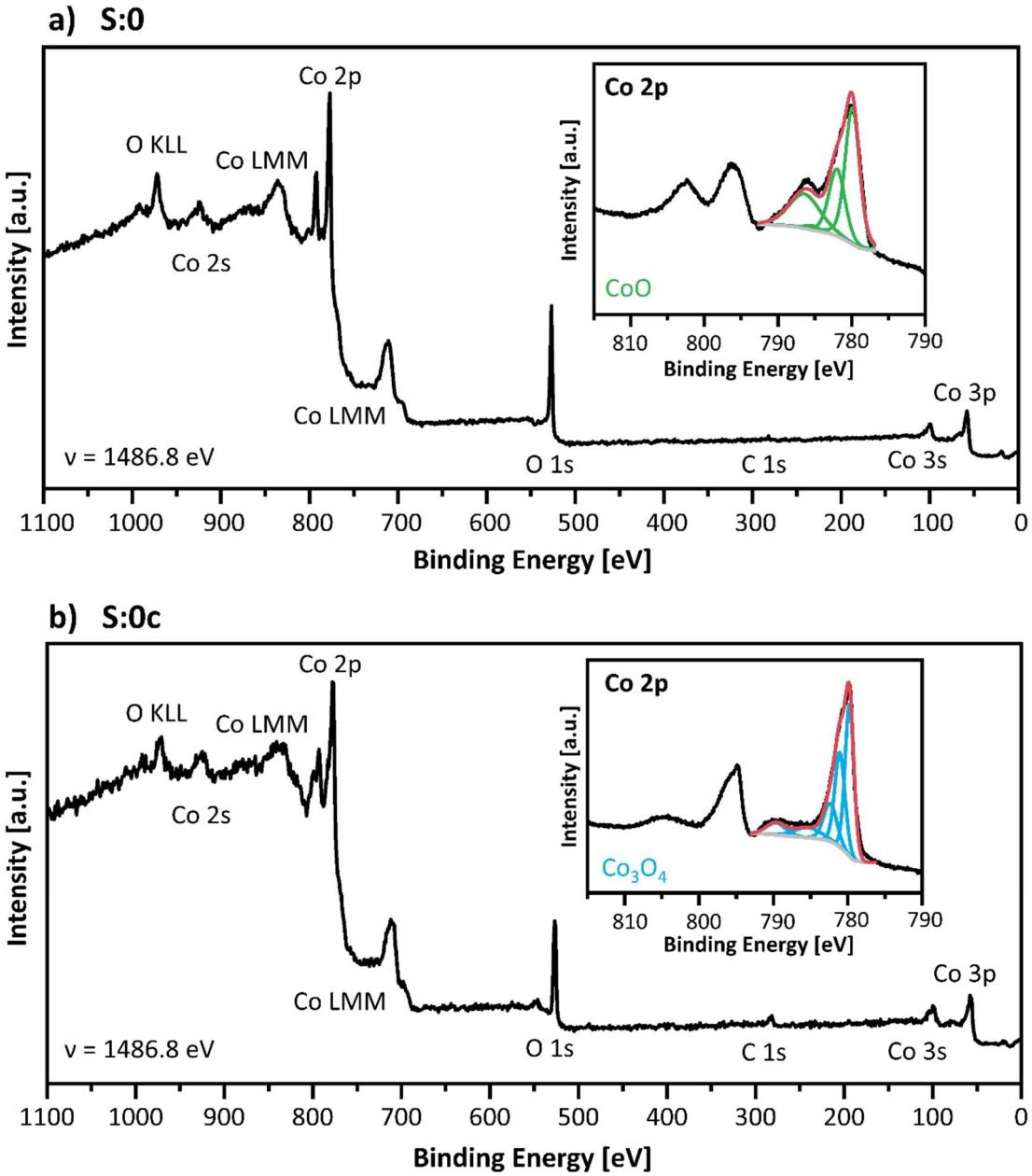

Figure S3. XPS measurements of S:0 (a) and S:0c (b). Inset: High resolution Co 2p spectra.

IV. FT-IR spectroscopy

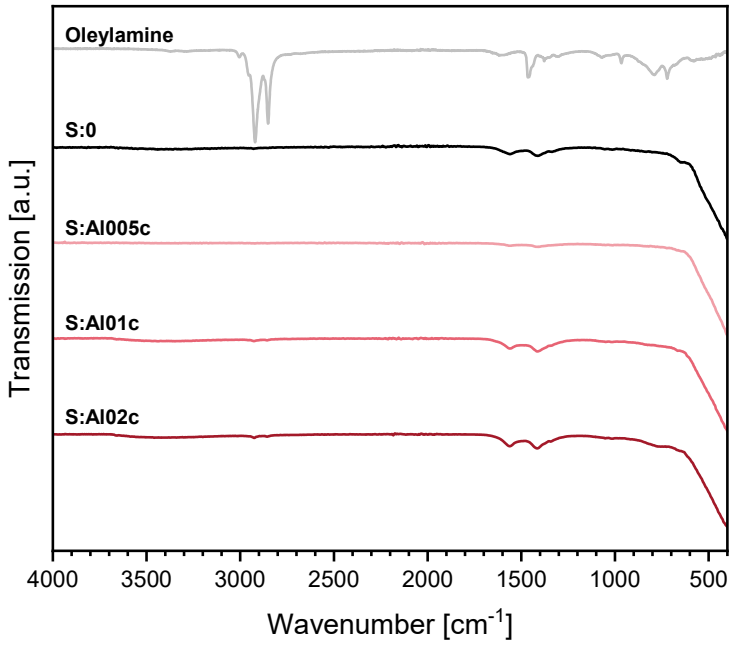

Figure S4. FT-IR measurements of uncalcinated samples S:0, S:Al005, S:Al01 and S:Al02 compared to oleylamine spectrum.

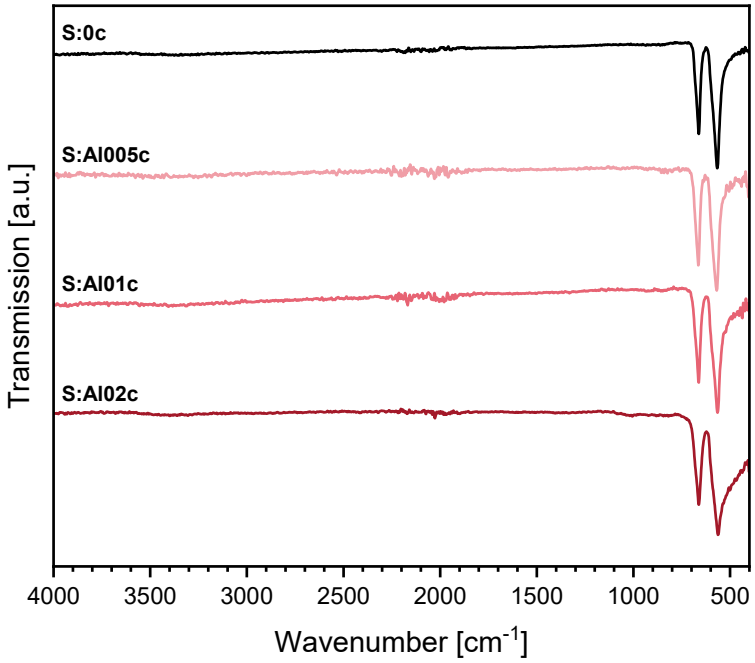

Figure S5. FT-IR measurements of calcinated nanoparticles S:0c, S:Al005c, S:Al01c and S:Al02c.

V. TEM Characterization

S:0c

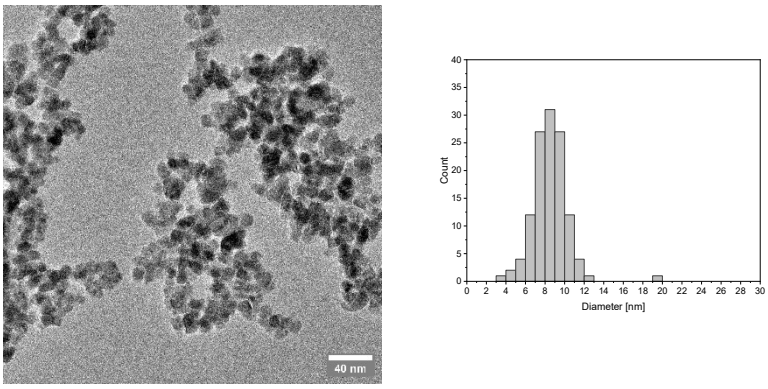

Figure S6. TEM image and particle size distribution of Co_3O_4 nanoparticles S:0c.

S:Al005c **S:Al01c** **S:Al02c**

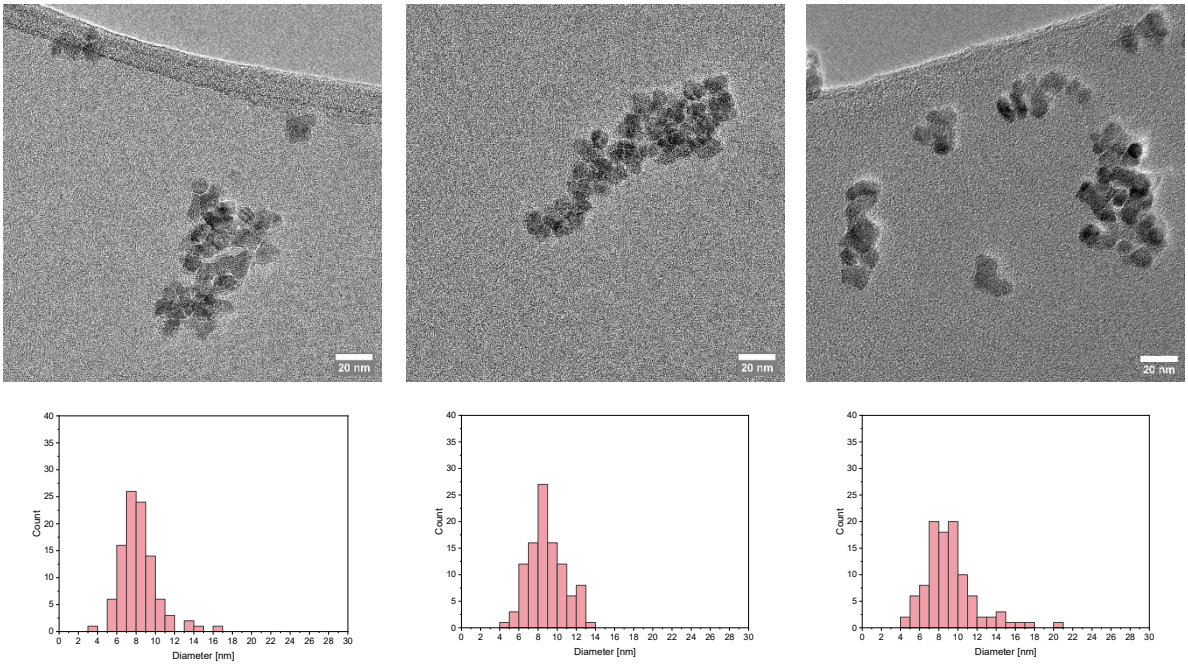

Figure S7. TEM images and particle size distribution of Al-doped Co_3O_4 nanoparticles.

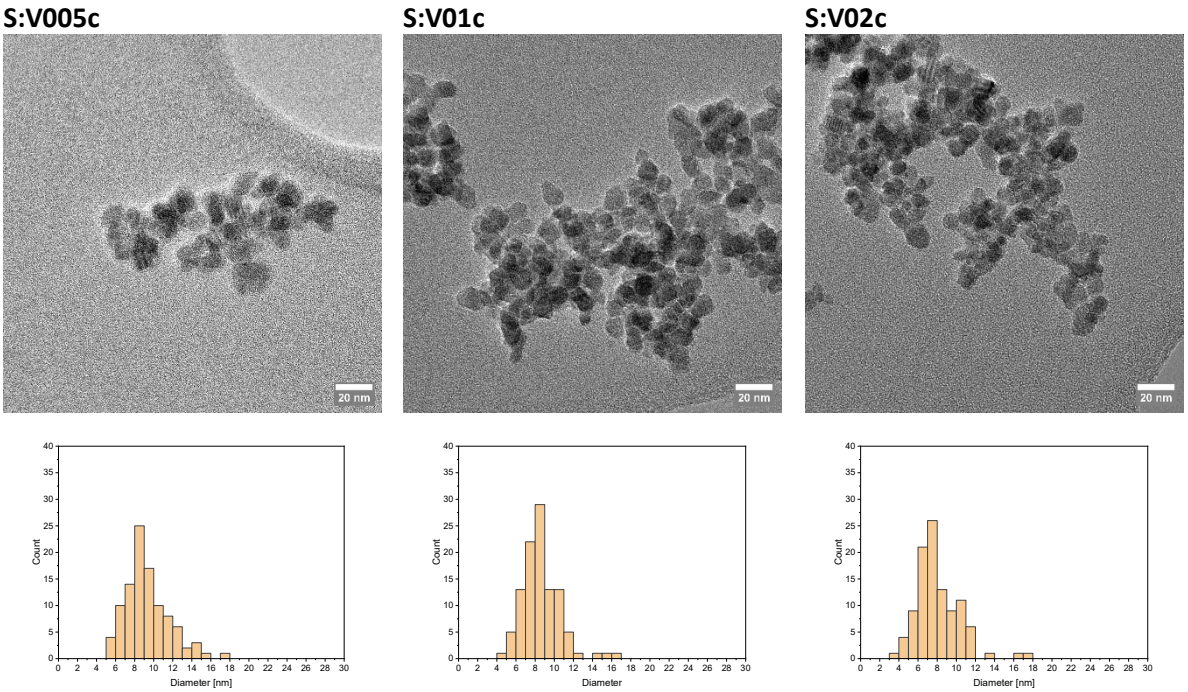

Figure S8. TEM images and particle size distribution of V-doped Co_3O_4 nanoparticles.

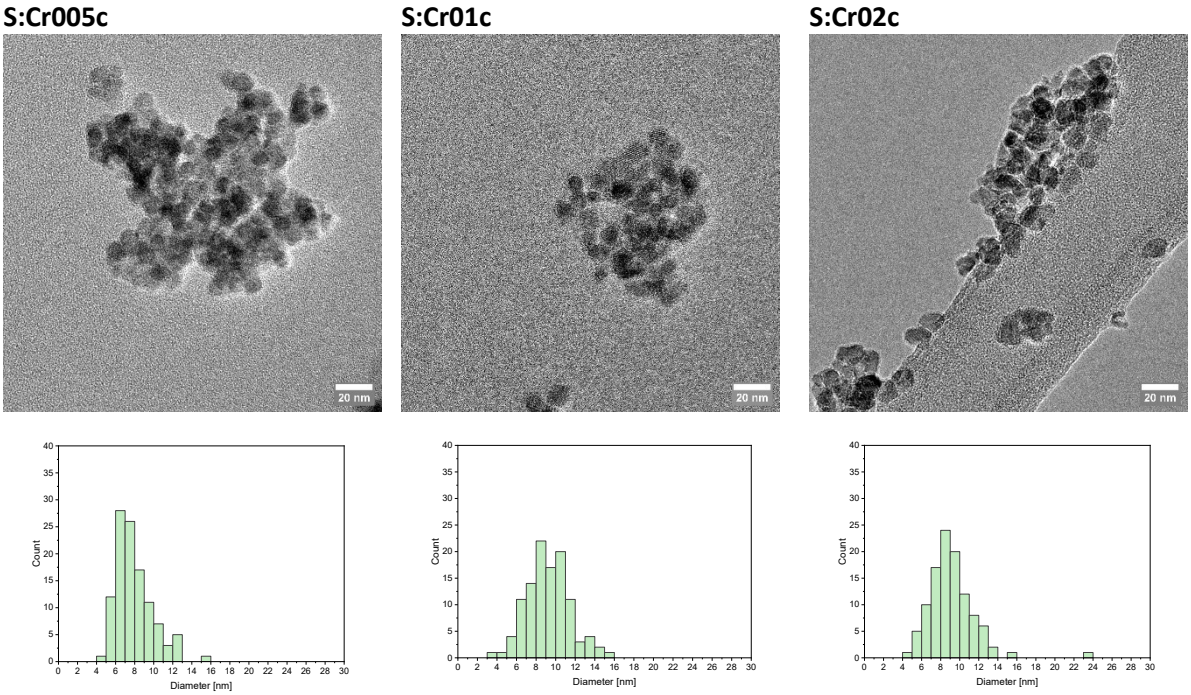

Figure S9. TEM images and particle size distribution of Cr-doped Co_3O_4 nanoparticles.

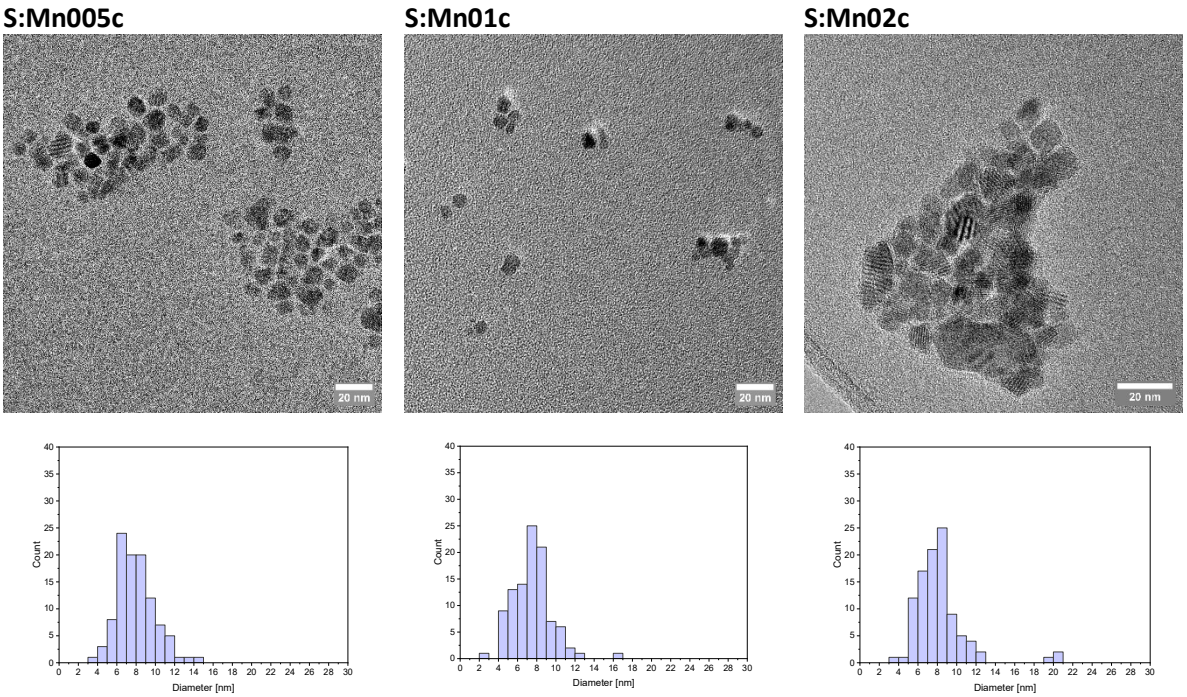

Figure S10. TEM images and particle size distribution of Mn-doped Co_3O_4 nanoparticles.

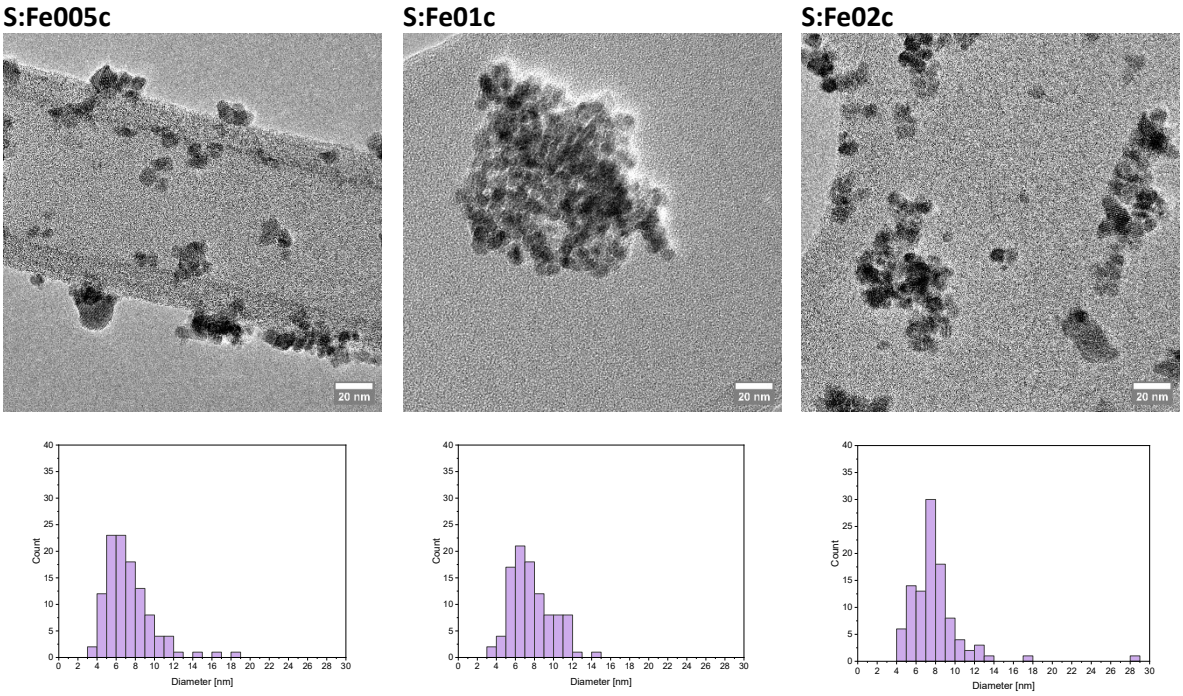

Figure S11. TEM images and particle size distribution of Fe-doped Co_3O_4 nanoparticles.

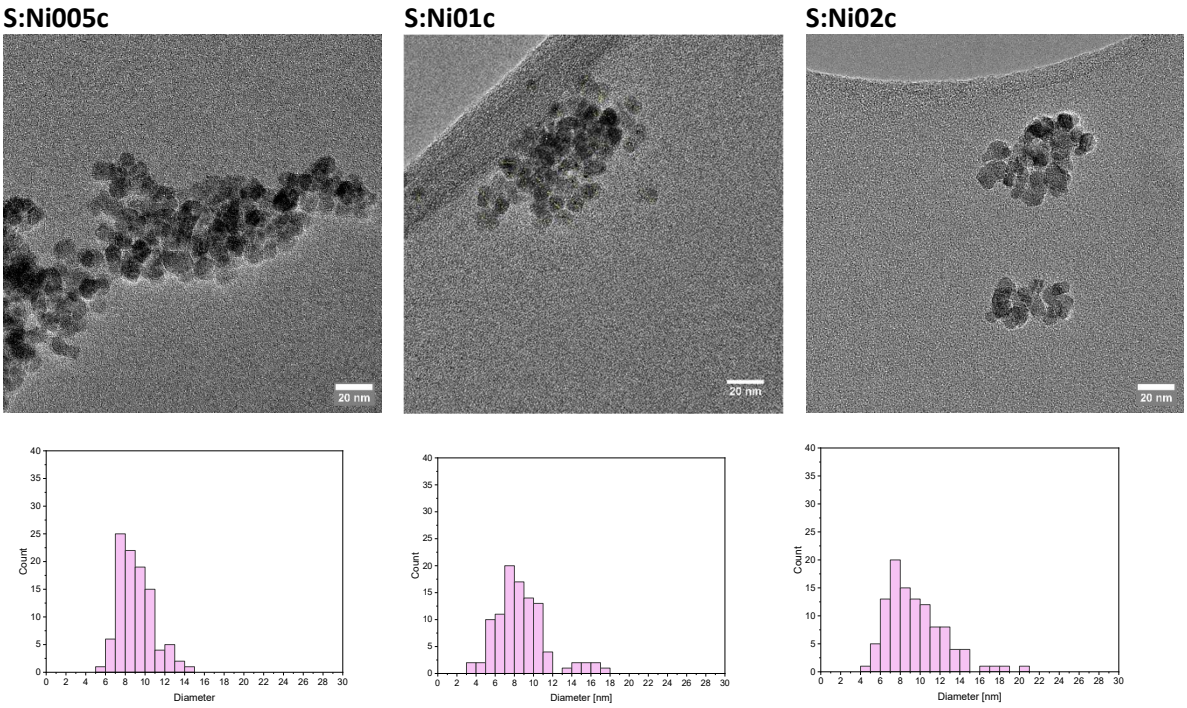

Figure S12. TEM images and particle size distribution of Ni-doped Co_3O_4 nanoparticles.

VI. EDX Characterization

Table S3. Metal concentration within the $M_{0.05}Co_{2.95}O_4$, $M_{0.1}Co_{2.9}O_4$ and $M_{0.2}Co_{2.8}O_4$ (M = Al, V, Cr, Mn, Fe, Ni) nanoparticle series determined by SEM-EDX bulk measurements.

	x = 0.05 [at%]	**x = 0.1 [at%]**	**x = 0.2 [at%]**
theoretical values	1.7	3.3	6.7
$Al_xCo_{3-x}O_4$	S:Al005c	S:Al01c	S:Al02c
	1.7	3.2	6.5
$V_xCo_{3-x}O_4$	S:V005c	S:V01c	S:V02c
	1.8	3.3	6.7
$Cr_xCo_{3-x}O_4$	S:Cr005c	S:Cr01c	S:Cr02c
	1.8	3.8	7.3
$Mn_xCo_{3-x}O_4$	S:Mn005c	S:Mn01c	S:Mn02c
	1.3	3.6	7.0
$Fe_xCo_{3-x}O_4$	S:Fe005c	S:Fe01c	S:Fe02c
	1.5	2.3	5.5
$Ni_xCo_{3-x}O_4$	S:Ni005c	S:Ni01c	S:Ni02c
	2.2	3.2	6.9

Sample S:Al02c

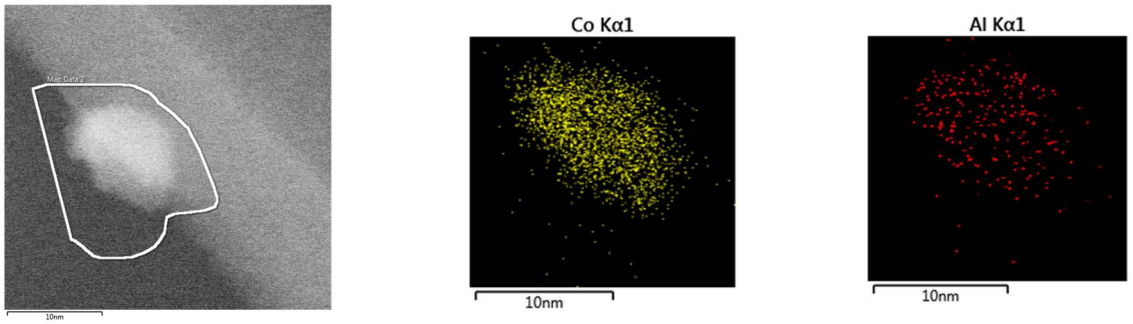

Figure S13. TEM-EDX Mapping of the Al-doped nanoparticle sample S:Al02c.

Sample S:V02c

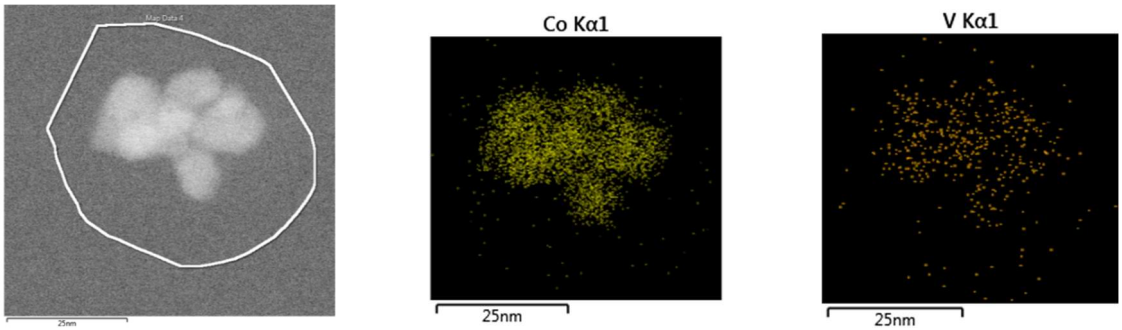

Figure S14. TEM-EDX Mapping of the V-doped nanoparticle sample S:V02c.

Sample S:Cr02c

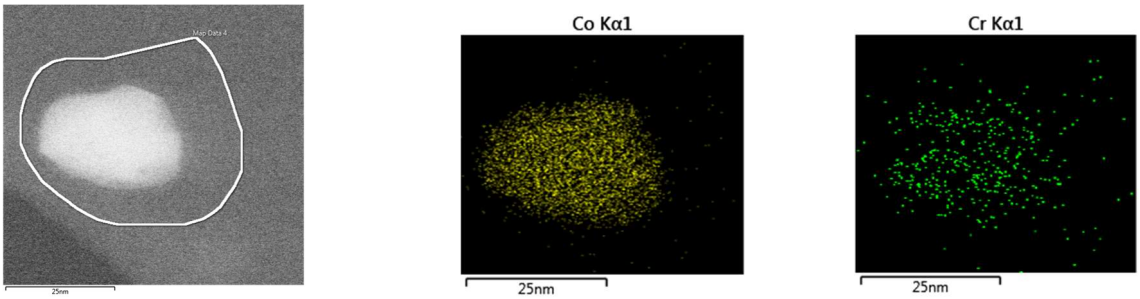

Figure S15. TEM-EDX Mapping of the Cr-doped nanoparticle sample S:Cr02c.

Sample S:Mn02c

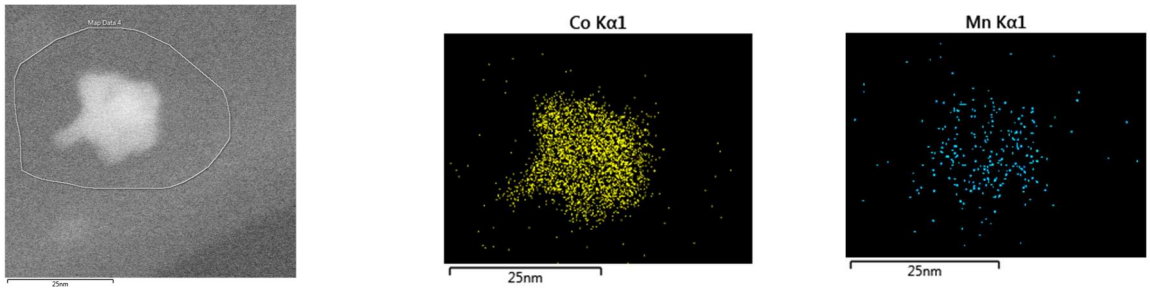

Figure S16. TEM-EDX Mapping of the Mn-doped nanoparticle sample S:Mn02c.

Sample S:Fe02c

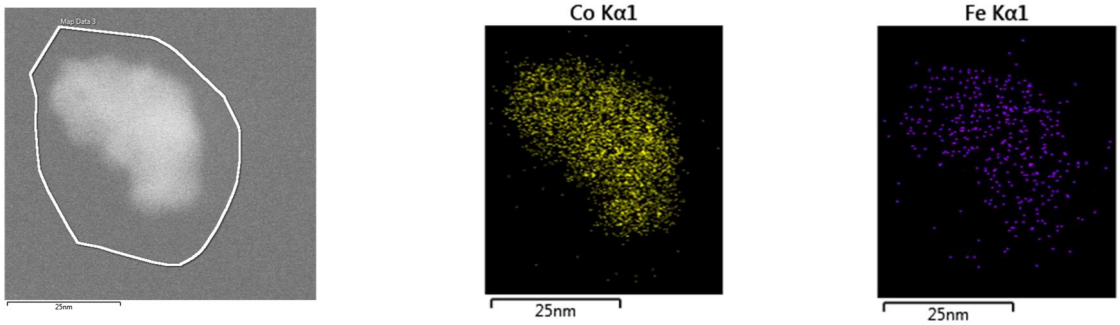

Figure S17. TEM-EDX Mapping of the Fe-doped nanoparticle sample S:Fe02c.

Sample S:Ni02c

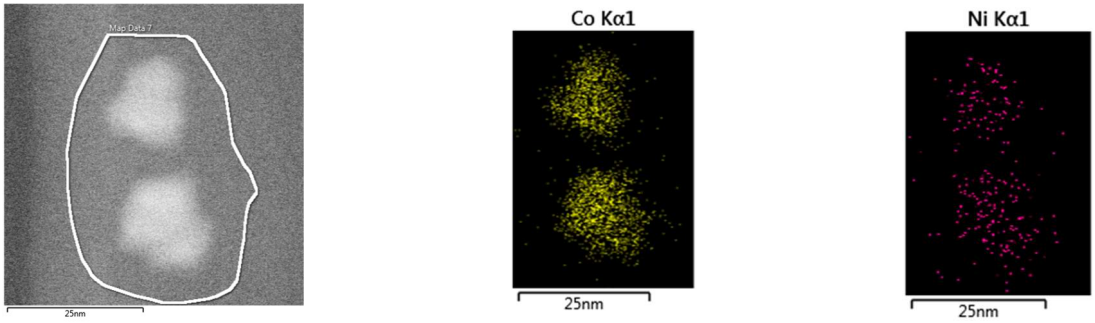

Figure S18. TEM-EDX Mapping of the Ni-doped nanoparticle sample S:Ni02c.

VII. Mössbauer spectroscopy

Mössbauer spectra were recorded on the Fe-containing samples (S:Fe005c, S:Fe01c, S:Fe02c) in order to discern the valency of the Fe-ions, as well as to characterize their overall electronic and magnetic state. The focus was on sample S:Fe02c since its higher Fe-content provided the highest signal intensity from the three samples that were characterized. The room temperature (300 K) spectrum revealed a doublet structure, indicating that the sample is in a paramagnetic state. After evaluation via a fitting routine (Figure S20a) we were able to determine an isomer shift δ of ca. 0.31 mm/s relative to α-Fe at room temperature, and a quadrupole splitting ΔE_Q of ca. 0.58 mm/s, indicating a high-spin Fe^{3+} state[1] with no Fe^{2+} being discernible within the detection limit, which usually exhibits far higher values of δ and ΔE_Q. A very slight asymmetry of the two lines could indicate a miniscule additional spectral contribution, which could not be resolved due to the overall low intensity.

At 5 K, the spectrum displays a magnetically ordered sextet state, which is to be expected due to the antiferromagnetic ordering in pure Co_3O_4 up to the Néel temperature $T_{Néel}$ of ca. 30 K.[2,3] Here, a non-Lorentzian line shape (reproduced by a narrow hyperfine field distribution) could indicate the presence of two subspectra in superposition, likely due to the distribution of Fe^{3+} on tetrahedral A-sites as well as octahedral B-sites. A broad sextet distribution is still present as a minor spectral component up to 80 K, indicating a slightly enhanced Néel temperature in S:Fe02c, matching trends in $T_{Néel}$ for $Fe_xCo_{3-x}O_4$ observed before.[3]

Due to the difficulties associated with the lower Fe content of samples S:Fe01c and S:Fe005c, only one spectrum was recorded at 80 K for each sample, to mitigate additional loss in spectral area by thermal excitation of phonons evident at higher temperatures. For these two, a pure paramagnetic doublet state is observed, consistent with lower values of $T_{Néel}$ closer to 30 K.

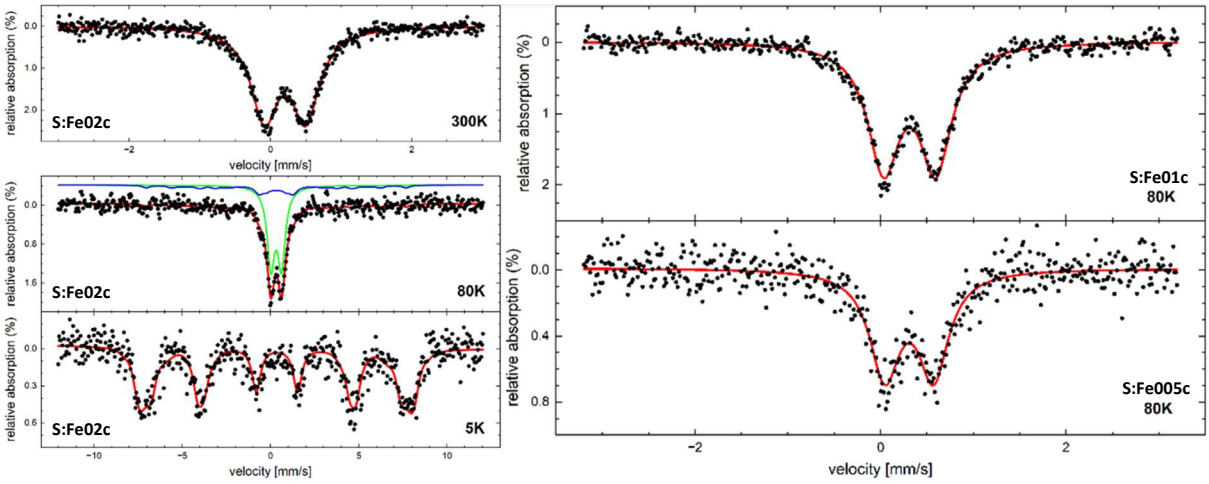

Figure S19. Mössbauer spectra of Fe-doped nanoparticles recorded between 5 and 300 K.

VIII. Electrochemical Characterization

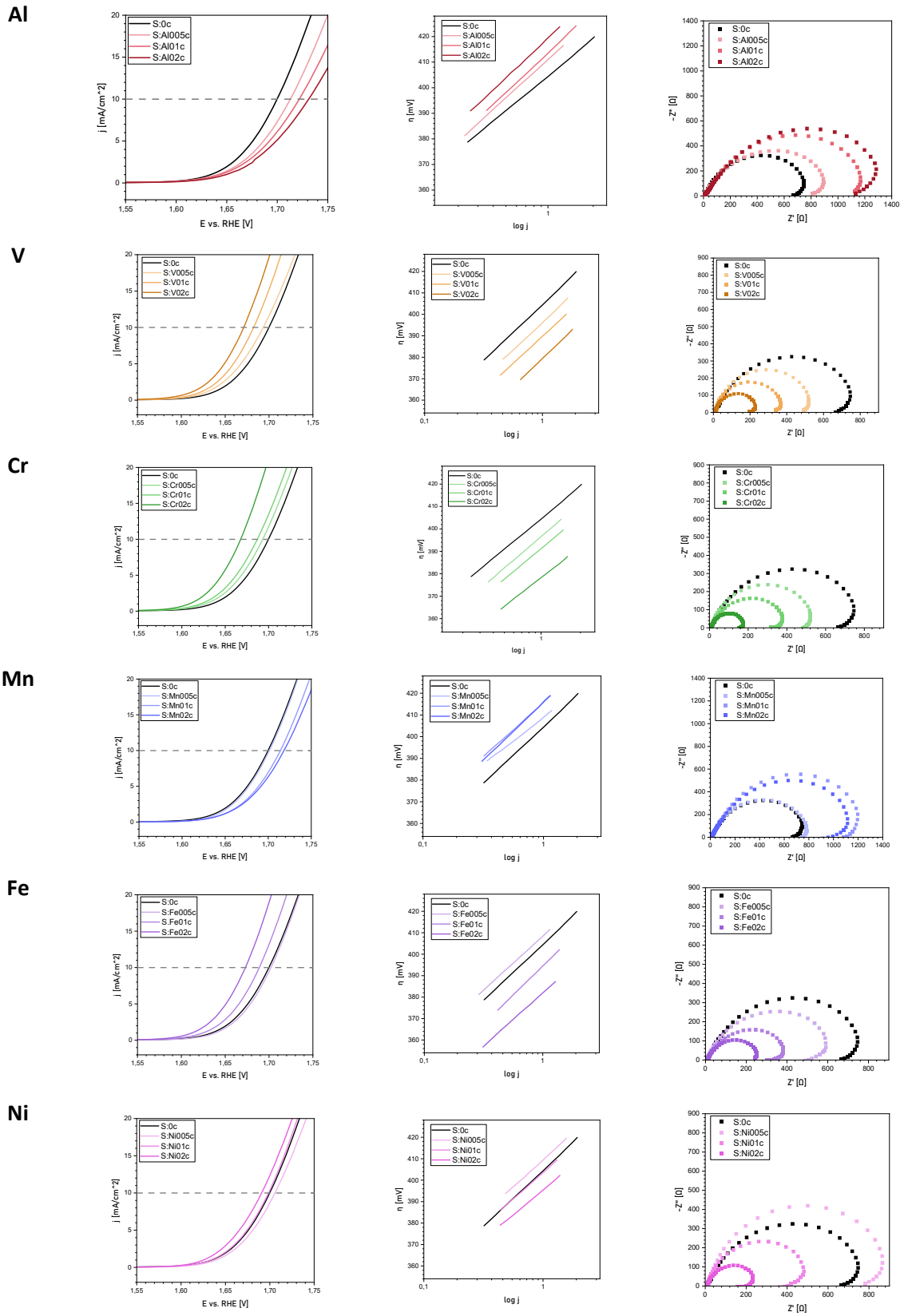

Figure S20. Electrochemical characterization of doped nanoparticles in comparison with pristine Co_3O_4 using LSV measurements, Tafel slope and EIS measurements.

IX. References

1 C. Gallenkamp, U. I. Kramm, J. Proppe and V. Krewald, *Int. J. Quantum Chem.,* 2021, 121:e26394.

2 Y. Ichiyanagi, Y. Kimishima and S. Yamada, *J. Magn. Magn. Mater.*, 2004, **272–276**, e1245.

3 M. Takahashi and M. E. Fine, *J. Appl. Phys.*, 1972, **43**, 4205.